Chemical Engineering Journal 470 (2023) 144024

Contents lists available at ScienceDirect

Chemical Engineering Journal

journal homepage: www.elsevier.com/locate/cej

Ratiometric SERS imaging for indication of peroxynitrite fluctuations in diabetic wound healing process

Hui Chen [a,b], Shanshan Lin [a,b], Dianqi Zhang [a,b], Yanlong Xing [a,b], Fabiao Yu [a,b,*], Rui Wang [a,b,*]

[a] Key Laboratory of Hainan Trauma and Disaster Rescue, The First Affiliated Hospital of Hainan Medical University, Hainan Medical University, Haikou 571199, China
[b] Engineering Research Center for Hainan Bio-Smart Materials and Bio-Medical Devices, Key Laboratory of Emergency and Trauma, Ministry of Education, Key Laboratory of Hainan Functional Materials and Molecular Imaging, College of Emergency and Trauma, Hainan Medical University, Haikou 571199, China

ARTICLE INFO

Keywords:
Surface-enhanced Raman scattering (SERS) imaging
Peroxynitrite fluctuation
Diabetes mellitus
Wound healing
Living cell and in vivo analysis

ABSTRACT

Peroxynitrite ($ONOO^-$) involves in diabetic wounds and its concentration is fluctuated in different pathological stages during the wound healing process. Thus, $ONOO^-$ may be utilized as a powerful biomarker to indicate the healing process of diabetic wound. However, the pathological roles of $ONOO^-$ can't be fully understood yet. Herein, inspired by the mechanism that phenylboronic pinacol ester can react with $ONOO^-$ specifically, we report a new kind of SERS nanoprobes to monitor $ONOO^-$ fluctuation during diabetic wound healing process. The gold-silver (Au@Ag) core-ultrathin shell nanoparticles were utilized as active substrate and conjugated with phenylboronic pinacol ester molecules on the surface of Ag shell to simultaneously act as Raman reporter molecules and recognition moiety of $ONOO^-$. In addition, functional polyethylene glycol (HS-PEG) and bovine serum albumin layers were sequentially immobilized on the surface of Ag shell to improve the stability of the nanoprobes. In the presence of $ONOO^-$, phenylboronic pinacol ester could be converted into the corresponding phenol, inducing the SERS signal changes. The concentration fluctuation of $ONOO^-$ could be quantitatively detected through the SERS signal intensity ratio (1076 cm^{-1}/998 cm^{-1}) changes of typical peaks. The nanoprobes exhibited a wide response range from 0 to 75 μM with 0.12 μM as the detection limit. In the diabetic wound skin models, $ONOO^-$ concentration fluctuations during the wound healing process before and after drug treatment could be obtained by SERS imaging. We expect the proposed SERS imaging assay could be a noninvasive and powerful tool to monitor the diabetic wound healing.

1. Introduction

Diabetes mellitus is one of the most common chronic diseases that severely threats human health, which is estimated to reach 784 million in 2045 according to the World Health Organization [1]. It has been confirmed that excessive ROS in vivo are closely related with chronic wound and wound repair due to the hyperglycemia environment [2,3]. The current clinical evaluation of wounds mainly relies on planimetry to quantitatively detect the changes of wound size, and granulation tissue formation [4]. The quantitative detection of biomarkers has been broadly applied to monitor the wound conditions, however, the detection is usually limited to laboratory testing, such as enzyme-linked immunosorbent assay (ELISA), which can't achieve to highly sensitive, noninvasive, in situ to monitor wound healing process [5].

During the diabetic wound healing process, the overexpressed ROS such as $O_2^{\bullet -}$ rapidly react with nitric oxide (NO) to produce peroxynitrite ($ONOO^-$) flux, which can induce the severe oxidative damage to the surrounding biological molecules including proteins and nucleic acids [6,7]. The previous researches indicate that $ONOO^-$ involves in diabetic wounds and its concentration is fluctuated in different pathological stages during the wound healing process [8–10]. Thus, $ONOO^-$ may be utilized as a powerful biomarker to indicate the healing process of diabetic wound. However, the pathological roles of $ONOO^-$ can't be fully understood yet. To explore its pathological roles in wound healing process, it's of great significance to develop noninvasive and sensitive detection technique to monitor the $ONOO^-$ fluctuations in the different pathological stages. Recently, a great many of analytical techniques have been utilized for the detection of $ONOO^-$ including colorimetric [11,12], electrochemical [13,14] and fluorescent assays [15–20]. However, colorimetric and electrochemical methods are difficult to be

* Corresponding authors at: Key Laboratory of Hainan Trauma and Disaster Rescue, The First Affiliated Hospital of Hainan Medical University, Hainan Medical University, Haikou 571199, China.
E-mail addresses: yufabiao@hainmc.edu.cn (F. Yu), wangrui@hainmc.edu.cn (R. Wang).

https://doi.org/10.1016/j.cej.2023.144024
Received 27 March 2023; Received in revised form 13 May 2023; Accepted 7 June 2023
Available online 8 June 2023

used for the measurement in living cells and in vivo. Although the fluorescent assay has been applied to detect $ONOO^-$ in living animals, it still suffered from the photobleaching and background inferences.

Surface-enhanced Raman scattering (SERS) has obtained more and more attention as a powerful analytical technique in biomedical detection, which not only provides fingerprint spectra of analytes but also possesses ultrahigh sensitivity, rapid response and specificity [21–24]. With these excellent properties, SERS has been utilized for sensing of various biological molecules and chemical reactions. Due to the ultrasmall Raman scattering cross-section, the inorganic molecules are difficult to be directly detected through SERS method. Fortunately, this shortcoming can be overcome by constructing specific reaction-based nanoprobes and observing the changes of typical Raman peaks before and after reactions [25–31].

Herein, inspired by the mechanism that phenylboronic pinacol ester can react with $ONOO^-$ specifically, we fabricated new SERS nanoprobes to monitor $ONOO^-$ fluctuation during diabetic wound healing process. The probes were composed of Au@Ag core-ultrathin shell nanoparticles as active substrate, conjugated with phenylboronic pinacol ester molecules on the surface of Ag shell, which simultaneously played the roles of Raman reporter and reaction moiety with $ONOO^-$. Furthermore, functional polyethylene glycol (HS-PEG) and bovine serum albumin (BSA) layers were sequentially immobilized on the surface of Ag shell to improve the stability of the probes. In the presence of $ONOO^-$, phenylboronic pinacol ester could be converted into the corresponding phenol, inducing the SERS signal changes. The concentration fluctuation of $ONOO^-$ could be quantitatively detected through the SERS signal intensity ratio (1076 cm^{-1}/998 cm^{-1}) changes of typical peaks. With all these features, we constructed the diabetic wound skin models using db/db mice and $ONOO^-$ fluctuation could be evaluated after drug treatment through highly sensitive SERS imaging. We expect the proposed SERS imaging assay could be a noninvasive and powerful tool to monitor the diabetic wound healing.

2. Experimental section

2.1. Materials and instruments

Mouse anti-3-nitrotyrosine (3-NT) monoclonal antibody (ab61392), rabbit anti-CD31 monoclonal antibody (ab76533), and rabbit anti-VEGF monoclonal antibody (ab32152) were purchased from Abcam (Shanghai, China). 3-NT ELISA kit, TNF-α ELISA kit, IL-1β ELISA kit and IL-6 ELISA kit were purchased from Elabscience (Wuhan, China). All the other reagents were from commercial sources with analytical grade and without any purification before use. The ultrapure water (18.2 MΩ·cm) was prepared by a Milli-Q water purification system (Billerica, MA, USA).

UV–vis absorption spectra were recorded using Nanodrop One microvolume spectrophotometer (Thermal Fisher, USA). The size distribution and zeta potential tests were performed using SZ-100Z2 particle size analyzer (Horiba, Japan). Transmission electron microscopy (TEM) images were obtained utilizing an HT7800 (Hitachi, Japan) system with an accelerating voltage of 120 kV. Raman measurements were performed using inVia Qontor Raman confocal microscope system (Renishaw, UK).

2.2. Preparation and characterization of SERS nanoprobes

Gold nanoparticles (Au NPs) were synthesized based on the previous research with minor modifications [32,33]. 20 μL, 2.5 mM of $AgNO_3$ was added to 2 mL of Au NPs solution and stirred for 2 h. Then, 20 μL, 1 mM of Raman reporter (4-(4,4,5,5-tetramethyl-1,3,2-dioxaborolan-2-yl) benzenethiol, MPBE) was dropped into the solution and vigorously stirred for 30 min. The solution color was changed from red to pink. Next, 100 μL, 0.2 mM of freshly prepared HS-PEG was introduced into the above solution and stirred for another 30 min. Subsequently, 10 μL, 10% BSA was introduced into the solution for 30 min. Finally, the solution was centrifuged (7000 rpm, 15 min) and resuspended in 1 mL ultrapure water to obtain the SERS probes stored solution. The properties of SERS probes were tested by UV–vis, DLS, TEM and SERS.

2.3. Cell culture

Mouse leukemia cells of monocyte macrophage (RAW 264.7) cell line was purchased from Procell in Wuhan, China. The cells were incubated in RPMI 1640 with 10% FBS. All the cells were cultured at 37 °C in a 95% humidified atmosphere with 5% CO_2.

2.4. Cytotoxicity of SERS probes

The cytotoxicity assessment of the SERS probes was confirmed by Cell Counting Kit-8 (CCK-8). The RAW 264.7 cells (5×10^4 cells/cell in 96-well plate) were incubated for 24 h at 37 °C under 5% CO_2. After introduction of different concentrations of SERS probes (0, 0.5, 1.0, 1.5, 2.0, 2.5, and 3.0 nM) and incubation for another 24 h, the cells were rinsed twice with PBS and CCK-8 solution was added to the wells. Then the optical density (OD) was recorded at 450 nm through a microplate reader (BioTek, USA). The cell viability was calculated through the following equations.

$$\text{Cell viability}(\%) = (\text{Mean OD of sample} \times 100)/(\text{Mean OD of the control group})$$

2.5. Intracellular SERS imaging in RAW 264.7 cells

2.5.1. Optimization of incubation time

SERS probes (1 nM) were incubated with RAW 264.7 cells for different time containing 6 h and 12 h. After washing for three times using PBS, the random single cell SERS imaging performed under 0.5 s, 633 nm and 50 × objective conditions.

2.5.2. SERS imaging of endogenous $ONOO^-$

SERS probes (1 nM) were incubated with RAW 264.7 cells for 12 h. Then, the culture medium containing the probe was removed and washed three times using PBS. The cells were treated with lipopolysaccharide (LPS, 1 μg/mL) and interferon-γ (IFN-γ, 50 ng/mL) for 4 h and then stimulated with phorbol-12-myristate-13-acetate (PMA, 10 nM) for 0, 0.5, 1, 2 and 3 h. The SERS imaging of three random cells was performed under 0.5 s, 633 nm and 50 × objective conditions.

2.5.3. SERS imaging of exogenous $ONOO^-$

SERS probes (1 nM) were incubated with RAW 264.7 cells for 12 h. Then, he culture dishes were washed three times using PBS to remove the unbound SERS probes. The cells were treated with 100, 400 μM of 3-morpholinosydnonimine hydrochloride (SIN-1) donor for 2 h, respectively. After washing three times with PBS, The SERS imaging of three random cells was performed under 0.5 s, 633 nm and 50 × objective conditions.

2.5.4. SERS imaging of single cell for monitoring $ONOO^-$ fluctuation

SERS probes (1 nM) were incubated with RAW 264.7 cells for 12 h.

Then, the culture dishes were washed three times using PBS to remove the unbound SERS probes. The RAW 264.7 cells were divided four groups as following: (a) Control group without any treatment; (b) LPS (1 μg/mL) and IFN-γ (50 ng/mL) were incubated with the cells for 4 h, followed by the stimulation with PMA (10 nM) for 3 h; (c) LPS (1 μg/mL) and IFN-γ (50 ng/mL) were incubated with the cells for 4 h, further stimulated with PMA (10 nM) for 3 h, and treated with the nitric oxide synthase inhibitor aminoguanidine (AG, 1 mM) for 0.5 h; (d) The cells were treated with SIN-1 (400 μM) for 2 h. SERS imaging of single cell was performed under 0.5 s, 633 nm and 50 × objective conditions.

2.6. Establishment of diabetic wound model

All animal experiments were performed in the animal experiment center of Hainan Medical University according to the experimental protocol approved by the Animal Protection Committee.

The db/db mice were first anesthetized using 3% pentobarbital with the dose of 10 μL/g. Then, the mice were exposed by removing the hair from their dorsum with a pet razor, a 0.5 cm diameter circular mark was made on the dorsum. After skin disinfection with 75 % alcohol, 5 mm biopsy perforations were made on each dorsum for excisional wound experiments. Wound pressure hemostasis and exposure treatments were performed and mice were housed in single cage. Trauma surgery was performed in an SPF level environment.

2.7. SERS imaging of diabetic wound model

Diabetic wound model mice were randomly divided into three groups (three mice per group): (1) untreated control, (2) treatment 1: bFGF, and (3) treatment 2: metformin + empagliflozin. In treatment groups, the wounded mice were treated with the drugs every day in the dose of bFGF (1 μg/mL) and metformin (250 mg/kg/d) + empagliflozin (10 mg/kg/d), respectively. Subsequently, 10 μL, 1 nM of SERS probe solution was sprayed on the wound surface to monitor the $ONOO^-$ fluctuations. Wounded mice with and without treatment were monitored for up to 14 days. The diameter of wounds was measured using a vernier caliper at the 1, 3, 5, 7, 10 and 14 day, and the wound area calculated as $\pi/4d^2$. SERS imaging was obtained on a Renishaw inVia Qontor Raman system under 633 nm of laser excitation, 8.5 mW of laser power, 0.5 s of acquisition time and 100 μm of step size. SERS imaging data was then processed using WIRE 5.3 software, and the Raman intensities at 998 cm^{-1} and 1076 cm^{-1} and ratio of 1076 cm^{-1}/998 cm^{-1} were presented. The wound skin tissues were collected and performed hematoxylin-eosin, Masson and immunohistochemistry staining tests.

2.8. Pilot toxicity evaluation

Blood samples were collected via tail vein and analyzed through a standard blood chemistry panel. The levels of inflammatory factors including 3-NT, TNF-α, IL-1β and IL-6 were detected using the corresponding ELISA kits. Major organs were collected for pathological examination of tissue sections.

3. Results and discussion

3.1. Pathophysiology of diabetic wound and SERS detection principle

Hyperglycemia will lead to pro-inflammatory state, neuropathy, tissue hypoxia and vascular function damage, which will have adverse effects on wound healing (Scheme 1). Hyperglycemia can also cause excessive glycosylation of protein and production of advanced glycosylation products, resulting in overexpression of pro-inflammatory cytokines, oxidative stress and changes in extracellular matrix. In addition, the chronic inflammatory environment in diabetes wounds, especially reactive oxygen species and protease, inhibits wound healing and tissue repair processes [34,35]. During the pathological process of wounded diabetic skin healing, the high concentration of NO and superoxide anion ($O_2^{\bullet -}$) produced in the body generate $ONOO^-$, which induces protein nitration. Therefore, $ONOO^-$ can be considered as a key

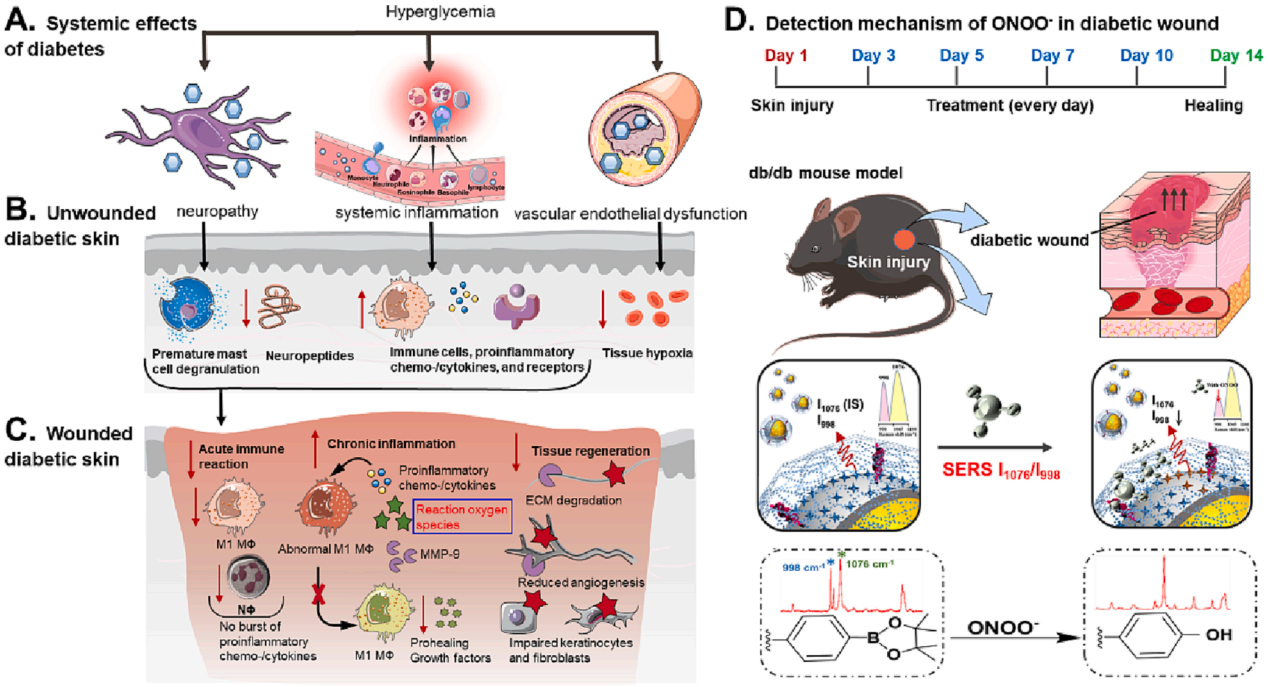

Scheme 1. Pathophysiology of diabetic wound healing and SERS detection of $ONOO^-$ for diabetic wound. (A) Systemic and (B) local diabetes-related physiological alternations in immune/ inflammatory response, cell/tissue function. (C) The reduced inflammatory response upon injury induces the chronic inflammation and lower tissue regeneration, especially the reaction oxygen species burst. (D) SERS detection of $ONOO^-$ in diabetic wound for healing monitoring. MΦ, macrophage. The illustrations were created with the help of BioRender.com.

indicator to monitor the process of wounded diabetic skin healing.

The SERS probes were fabricated by assembling the MPBE molecules on the surface of Au@Ag core–shell NPs, followed by the function of mercapto-polyethylene glycol (HS-PEG) and bovine serum albumin (BSA) to improve the stability. Here, Au@Ag core–shell NPs were selected as the SERS substrate. Considering the potential interference of Ag shell toward $ONOO^-$ detection, ultrathin Ag shell introduced through controlling the amount of silver nitrite ($AgNO_3$). The phenylboronic pinacol ester exhibited much higher reaction rate with $ONOO^-$ compared to the conversion to the corresponding phenylboronic acid in solution at pH = 7.4. Accordingly, the phenylboronic pinacol ester has great potential to be used as the key moiety to detect $ONOO^-$ in physiological environment. Upon reaction with $ONOO^-$, the boronic pinacol ester groups of the probes will turn into phenol groups, inducing the significant typical peak changes of SERS probes. The ordinary SERS probes usually use the Raman signal of single peak to quantitatively measure the target, however, the detection reliability will be affected by uncontrollable factors. To overcome these shortcomings, ratiometric method based on signal intensity changes of typical peaks is often utilized in SERS detection, which can reduce background interference and significantly improve the reliability and stability of SERS probes. Therefore, the Raman intensity ratio of I_{1076}/I_{998} was selected for quantification of $ONOO^-$ levels in living cells and diabetic wound.

3.2. Optimization of SERS probes

Au@Ag core–shell NPs were used as SERS active substrate, and MPBE molecules played the dual roles of Raman reporter and recognition moiety of $ONOO^-$. Here, the gold core nanoparticles were coated by ultrathin silver shell, which could simultaneously preserve the plasmonic properties of gold nanoparticles and provide the silver as the external shell. To improve the stability of the probe, HS-PEG and BSA

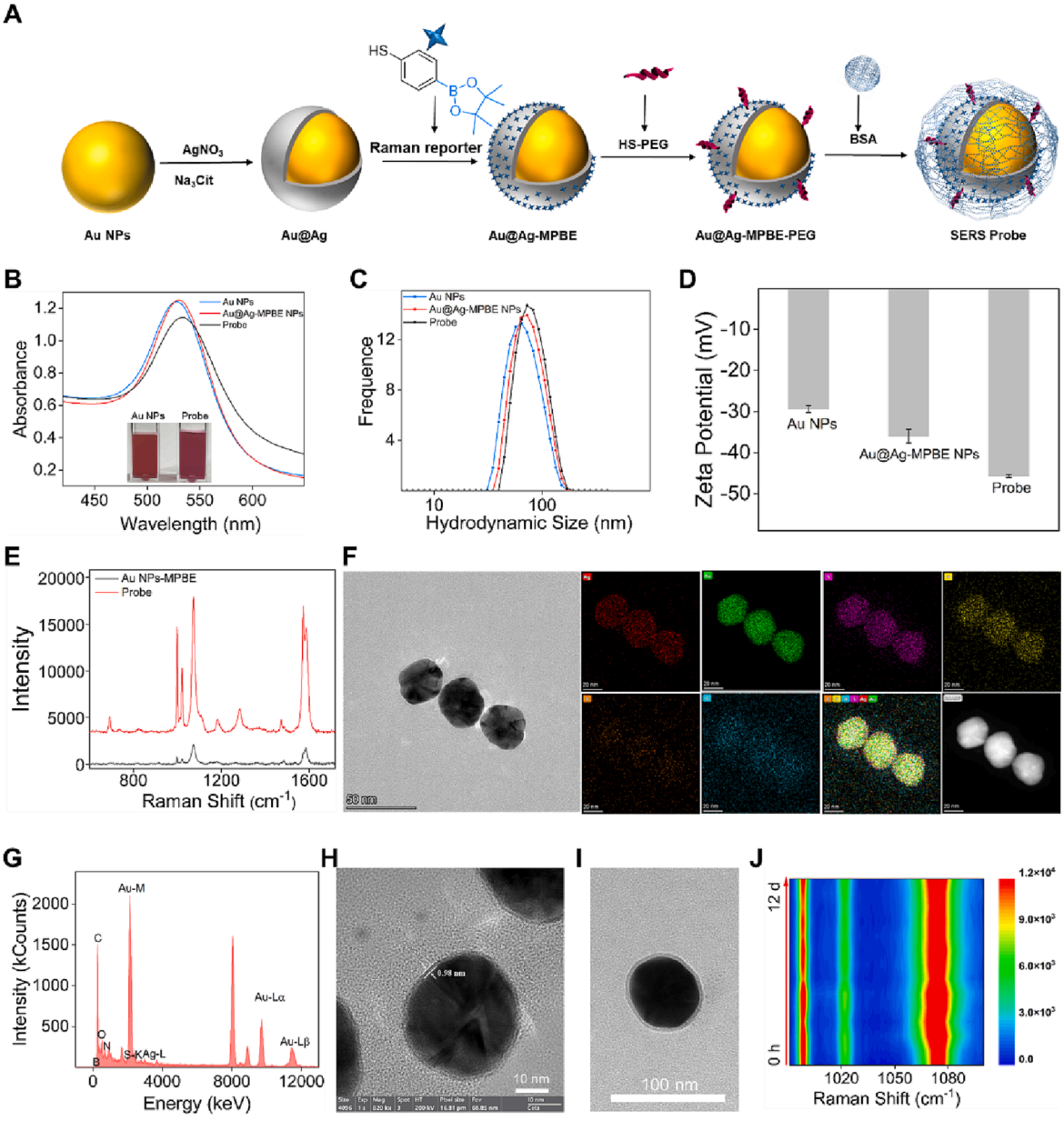

Fig. 1. Preparation and characterization of SERS probes. (A) The preparation protocol of SERS probes. (B) UV–vis spectra of SERS probe and precursor nanoparticles, insert: photographs of Au NPs and probes. (C) DLS distributions. (D) Zeta potential. (E) SERS spectra of Au NPs and probes. (F-G) HAADF-STEM and EDS elemental maps of SERS probes. (H) TEM image of Au@Ag NPs displays the ultrathin silver shell. (J) TEM image of probe indicates the BSA shell. (J) Stability test of SERS signal intensity of SERS probes within 12 days.

were sequentially decorated on the surface of silver shell after modifying MPBE molecules (Fig. 1A). Correspondingly, UV–vis spectra exhibited the red shift from 528 nm to 535 nm as shown in Fig. 1B. In addition, size distribution and zeta potential indicated an increase size and lower potential value of SERS probe compared to Au NPs (Fig. 1C and D). In contrast, the SERS signal intensity of the probe was significantly enhanced due to the introduction of ultrathin silver shell. The formation of ultrathin silver shell was confirmed through high-angle annular dark field-scanning/transmission electron microscopy (HAADF-STEM). In addition, energy dispersive spectra (EDS) were used for elemental analysis of the SERS probe. In addition, high-resolution TEM images confirmed that the thickness of silver shell was about 1 nm and the formation of BSA shell (Fig. 1H and I). The stability of SERS probes usually affects the detection of the targets in the biological and physiological environment. The stability of SERS signal intensities at 998 cm^{-1} and 1076 cm^{-1} were investigated within 12 days in fetal bovine serum (FBS). Fortunately, there were no significant changes, indicating the excellent stability and capability utilizing in the biological milieu (Fig. 1J).

3.3. $ONOO^-$ responses of SERS probes in the solution

The selectivity, cytotoxicity, dynamic response and sensitivity of the probe are the key parameters to achieve highly sensitive and specific detection of $ONOO^-$. Since the possible interferences causing by the complex matrices usually affect the detection specificity, therefore, various relevant biological species were tested to confirm the specificity of the proposed probe. As shown in Fig. 2A, only $ONOO^-$ could trigger the changes of ratio of I_{1076}/I_{998}, while other species could not induce the significant changes of ratio even at much higher concentration than $ONOO^-$ after incubation for 3 min, demonstrating the excellent selectivity. In order to investigate the cytotoxicity of the probe, cell counting kit-8 was utilized to measure the cell viability after incubation of the probe and RAW 264.7 cells for 24 h. The cell viability still remained more than 85%, which indicated the probe had good biocompatibility and had the potential to be used in the living cells (Fig. 2B). Due to the strong oxidation ability and rapid reaction rate with phenylboronic pinacol ester group of $ONOO^-$, the incubation time of the probe and $ONOO^-$ was carefully investigated within 2 min as shown in Fig. 2C and D. The probe (1 nM) was incubated with $ONOO^-$ (50 μM) and the SERS spectra were recorded at different time points. The ratio of I_{1076}/I_{998} reached the maximum after reaction for 90 s, while the ratio values decreased after 90 s. This phenomenon could be attributed to the cleavage of Ag-S bond between silver shell and MPBE molecules due to the strong oxidation ability of $ONOO^-$. Thus, 90 s was utilized as the optimized reaction time for the detection of $ONOO^-$.

Next, the response of various concentrations of $ONOO^-$ (0, 5, 7.5, 10, 20, 30, 40, 50, 75 and 100 μM) toward SERS probes were performed. After reaction for 90 s for each concentration, their SERS spectra were obtained as shown in Fig. 2E. The SERS intensity ratio of I_{1076}/I_{998} of MPBE was used for quantitative evaluation of $ONOO^-$. Consequently, with the concentration of $ONOO^-$ increasing, the SERS signal intensity ratio was concomitantly increased until the concentration of $ONOO^-$ reached 75 μM. After that, the ratio value significantly decreased due to the cleavage of Ag-S bond. On the basis of SERS signal intensity ratio of I_{1076}/I_{998}, the calibration curve for the quantitative evaluation of $ONOO^-$ was constructed as shown in Fig. 2F, which was determined from the sigmoidal function. Furthermore, the probe exhibited a wide response range from 0 to 75 μM with 0.12 μM as the detection limit, demonstrating the ability of sensitive detection of $ONOO^-$ in solution and great potential in biological systems.

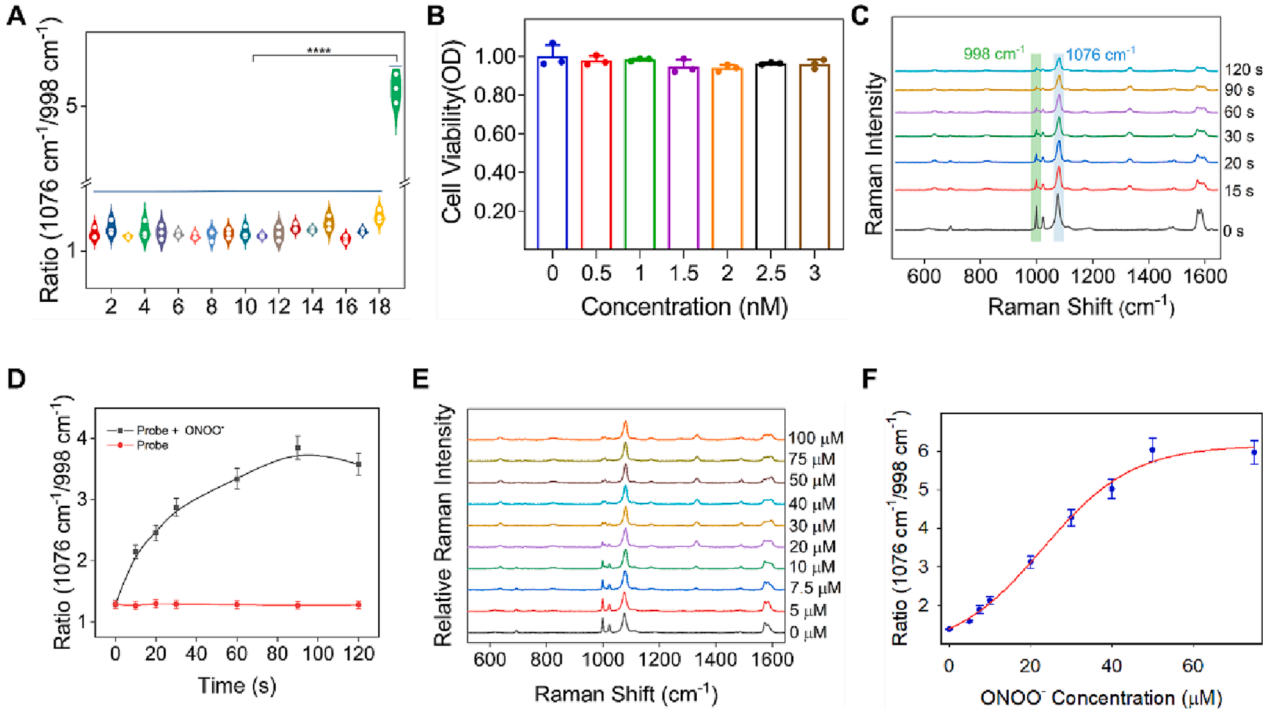

Fig. 2. (A) Raman intensity ratio (I_{1076}/I_{998}) of SERS probe (1 nM) in the presence of various ROS, RNS and other analytes within 3 min. 1. PBS control; 2. $MgSO_4$; 3. $CuSO_4$; 4. KCl; 5. Na_2CO_3; 6. Na_2SO_4; 7. Na_2S; 8. $CaCl_2$; 9. $ZnSO_4$; 10. $NaHSO_3$; 11. GSH; 12·H_2O_2; 13. ClO^-; 14. AchE; 15. $O_2^{\bullet-}$; 16. NO; 17. OH^- (2–17 100 μM); 18. L-Cys (300 μM); 19. $ONOO^-$ (50 μM). (B) Cell viability of the SERS probe against RAW 264.7 cells. (C) Time-dependent SERS spectra and corresponding Raman intensity distribution at I_{1076}/I_{998} of the probe toward $ONOO^-$ (50 μM) acquired at 2 min. (D) Raman intensity ratio of I_{1076}/I_{998} corresponding to (C). (E) Changes of the Raman intensity of probe (1 nM) incubated with an increasing concentration of $ONOO^-$ (0–100 μM). (F) Corresponding calibration line of Raman intensity ratio of I_{1076}/I_{998} as a function of the sigmoidal of the concentration of $ONOO^-$. All spectra were measured in PBS containing 20% FBS (20 mM, pH 7.4, v/v, 633 nm-laser power, 1 s exposure time). Statistical analysis was performed using one-way analysis of variance followed by post hoc Tukey multiple comparisons (n = 3, mean ± S. E. M., ***P < 0.001).

3.4. Cellular SERS detection of $ONOO^-$

To explore the feasibility of SERS probe for detecting intracellular $ONOO^-$ and the optimized incubation time between SERS probe and RAW 264.7 cells, the probe was entered into the cells through endocytosis. After incubation for 6 and 12 h, respectively, the TEM images and SERS imaging were performed. TEM images exhibited that the probe was mainly distributed in the cytoplasm, providing the located sites of the probes. In addition, TEM images also confirmed that 12 h of incubation time showed better endocytosis efficacy for the probe. Upon incubation, SERS imaging of five random cells was performed, providing higher Raman signal intensity and intensity ratio of 1076 cm^{-1}/998 cm^{-1} after 12 h than that of 6 h as shown in Fig. 3. These results demonstrated that 12 h was the optimized incubation time to provide excellent SERS signals.

To further explore the biosensing application, the performances of the probe in RAW 264.7 cells were also investigated by detecting endogenous and exogenous $ONOO^-$. The numerous previous researches have confirmed that $ONOO^-$ is produced through the reaction of NO and$O_2^{\bullet -}$, which can be produced from L-arginine by NO synthetase and from O_2 by xanthine oxidase, respectively. Upon stimulation with LPS, IFN-γ and PMA, the living cell will produce excessive NO and ROS. On the other hand, SIN-1 is considered to be an $ONOO^-$ releasing compound. Therefore, we investigated the $ONOO^-$ concentration fluctuations under the two factors. The first factor was changing the stimulation time of PMA. The RAW 264.7 cells were pretreated with LPS (1 μg/mL) and IFN-γ (50 ng/mL) for 4 h, then stimulated using PMA (10 nM) for 0 to 3 h. SERS imaging of three random cells under each condition was performed as shown in Fig. 4A. The mean ratios of I_{1076}/I_{998} exhibited a raising tendency with the increasing PMA stimulation time due to the production of more $ONOO^-$ induced by higher concentration of O2 under longer PMA stimulation time. Thus, 3 h was selected as the optimized PMA stimulation time. We also investigated the effect of different concentrations of SIN-1. As indicated in Fig. 4B, the ratio of I_{1076}/I_{998} at the concentration of 400 μM was much higher than that of 100 μM after incubation for 2 h of RAW 264.7 cells and SIN-1. Accordingly, 400 μM was selected as the optimized concentration of SIN-1. Interestingly, as shown in Fig. 4C and D, the coefficients of variation of ratio of I_{1076}/I_{998} in both groups were<10%, indicating the very small difference among the three random cells under the same conditions, which demonstrated that the single-cell SERS imaging was available.

Single-cell SERS imaging can collect the separate data from individual cells, as opposed to values averaged over populations of cells, which presents the more precise analysis. Ratio of I_{1076}/I_{998} utilized for SERS imaging of $ONOO^-$ remained low level in the SERS image of a single RAW 264.7 cell containing SERS probes without stimulation (Fig. 5A, group a), probably because the endogenous $ONOO^-$ in normal RAW 264.7 cells was not enough to trigger reactions. However, the significantly increased signals of I_{1076}/I_{998} could be observed after stimulation with LPS, IFN-γ and PMA, indicating the generation of higher concentration of $ONOO^-$ under the stimulation. To confirm that the SERS response in group b originated from $ONOO^-$ in the living cells, a control experiment was conducted by treating the SERS probe-contained cells with AG, a nitric oxide synthase inhibitor, along with LPS, IFN-γ and PMA stimulation. As expected, the ratio of I_{1076}/I_{998} decreased the low levels as well as the group a, implying that the inhibition of NO synthase using AG induced less production of $ONOO^-$ in the living cells (group c). Moreover, SIN-1 was introduced into the SERS probe-contained cells and the increased ratio of I_{1076}/I_{998} could be observed. These results demonstrated that the proposed SERS probe could achieve highly sensitive and specific detection of endogenous and exogenous $ONOO^-$ in living cells.

3.5. Evaluation of diabetic wound healing

The diabetic wounded skin models were constructed using db/db mice, which were divided into three groups. The mice without any treatment were selected as the control group. The treatment groups using basic fibroblast growth factor (bFGF) and metformin + empagliflozin were selected as the treatment 1 and treatment 2 groups, respectively. Fig. 6A illustrated the $ONOO^-$ fluctuations during the wound healing progress in the three groups of diabetic mice before and after treatment. The photographs of the wound sites and size changes were recorded until 14 days, at which time the tissues were collected for histological evaluation. The size changes after 14 days revealed the healing rate with incomplete scabs was much lower in control group than that of other two treatment groups. However, the wound in the treatment groups exhibited much smaller areas, which was attributed to the strong angiogenic effect in treatment 1 group and reduced level of inflammation due to the lower blood sugar in treatment 2 group (Fig. 6B). To further determine the $ONOO^-$ fluctuation during the

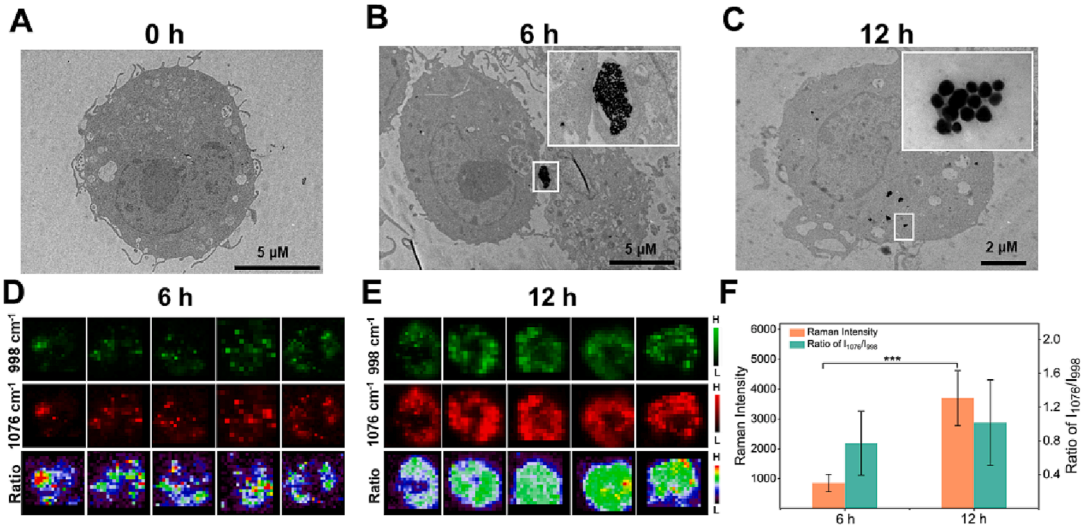

Fig. 3. (A–C) TEM images of RAW 264.7 cells incubated with probe (1 nM) for 0 h, 6 h and 12 h, respectively. (D) and (E) Intracellular SERS mapping images of five random RAW 264.7 cells incubated with probe (1 nM) for 6 h and 12 h, respectively. (F) Mean Raman signal intensity and intensity ratio (I_{1076}/I_{998}) of five random cells in (D) and (E). Single-cell SERS mapping was achieved using exposure time of 0.5 s (633 nm-laser power, 50 × objective). Statistical analysis was performed using one-way analysis of variance followed by post hoc Tukey multiple comparisons (n = 5, mean ± S. E. M., ***P < 0.001).

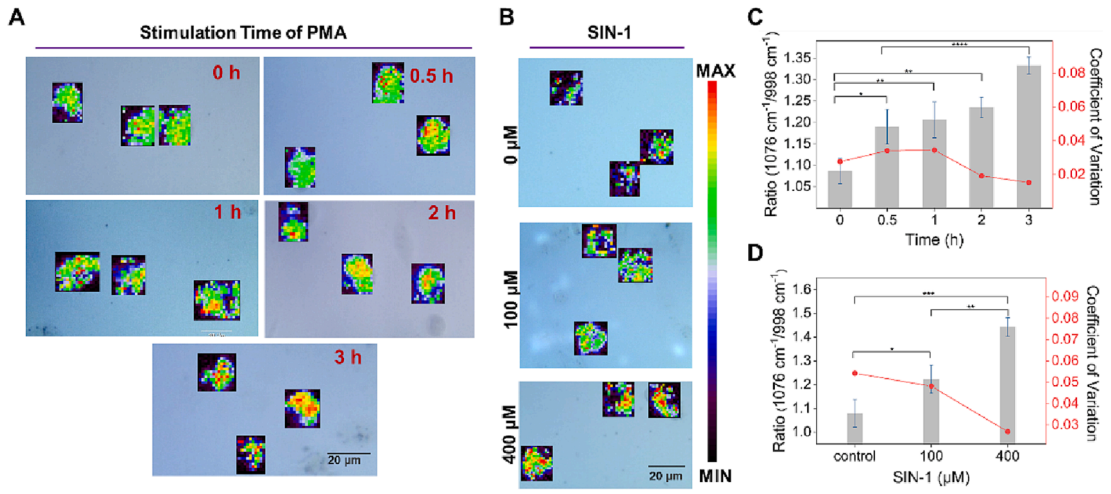

Fig. 4. (A) SERS mapping images after stimulation with PMA (10 nM) for 0 h, 0.5 h, 1 h, 2 h and 3 h, respectively. (B) SERS mapping images after pretreatment with different concentrations of $ONOO^-$ donor SIN-1 (0, 100 and 400 μM). (C) and (D) Statistical analysis of Raman intensity ratio of I_{1076}/I_{998} in (A) and (B), respectively. Single-cell SERS mapping was achieved using exposure time of 0.5 s (633 nm-laser power, 50 × objective). Statistical analysis was performed using one-way analysis of variance followed by post hoc Tukey multiple comparisons (n = 3, mean ± S. E. M., *P < 0.05, **P < 0.01, ***P < 0.001, ****P < 0.0001).

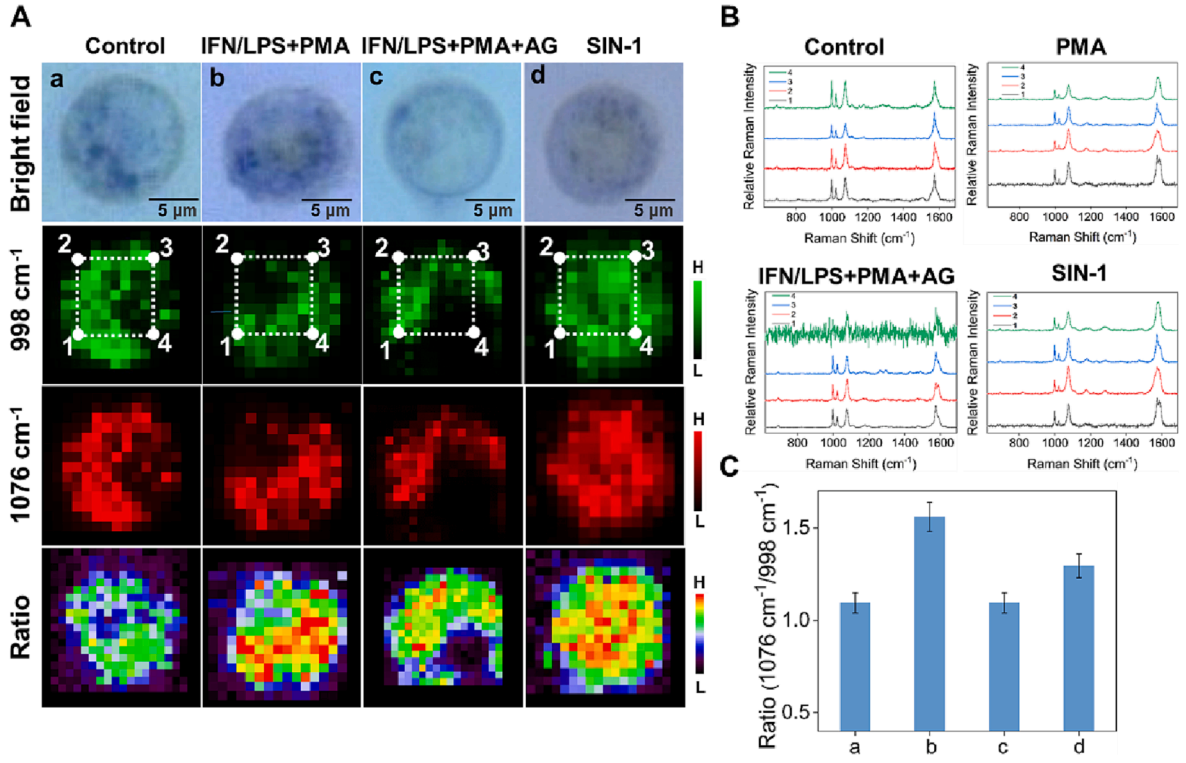

Fig. 5. (A) Single-cell SERS mapping images of RAW 264.7 cells. These cells were pretreated with the probe (1 nM) for 12 h. (a) PBS control group; (b) cells were incubated with LPS (1 μg/mL) and IFN-γ (50 ng/mL) for 4 h and then PMA (10 nM) for 3 h in the culture medium; (c) cells were pretreated with LPS (1 μg/mL) and IFN-γ (50 ng/mL) for 4 h, then PMA (10 nM) for 3 h and AG (1 mM) for 30 min in the culture medium; (d) cells were incubated with ONOO– donor SIN-1 (400 μM) for 2 h. (B) SERS spectra of the different positions in (A). (C) Quantification of Raman signal intensity ratio of I_{1076}/I_{998} in (A). Single-cell SERS mapping was achieved using exposure time of 0.5 s (633 nm-laser power, 50 × objective).

diabetic wound healing process, SERS imaging based on our proposed probe was recorded for up to 14 days after with and without treatment on the wound. Strong SERS ratio signals were collected all over the wound area on 1st day, indicating the high concentration of $ONOO^-$ at the early stage of wounds (Fig. 6C–E). To accelerate the wound healing process, bFGF was dropped on the surface of the wound to mediate the formation of new blood vessels (Fig. 6D). In addition, the combined application of metformin and empagliflozin could efficiently control the concentration of blood sugar on the normal level, which could reduce the oxidative stress and inflammation. After treatment, SERS imaging for each group was performed to evaluate the $ONOO^-$ concentration at 1st, 3nd, 5th, 7th, 10th and 14th day. Compared to treatment 2 group, the $ONOO^-$ concentration in treatment 1 group was much lower since the strong angiogenic effect of bFGF could efficiently reduce the inflammation. However, control group exhibited the higher ratio values of I_{1076}/I_{998} than other two treatment groups due to the serious

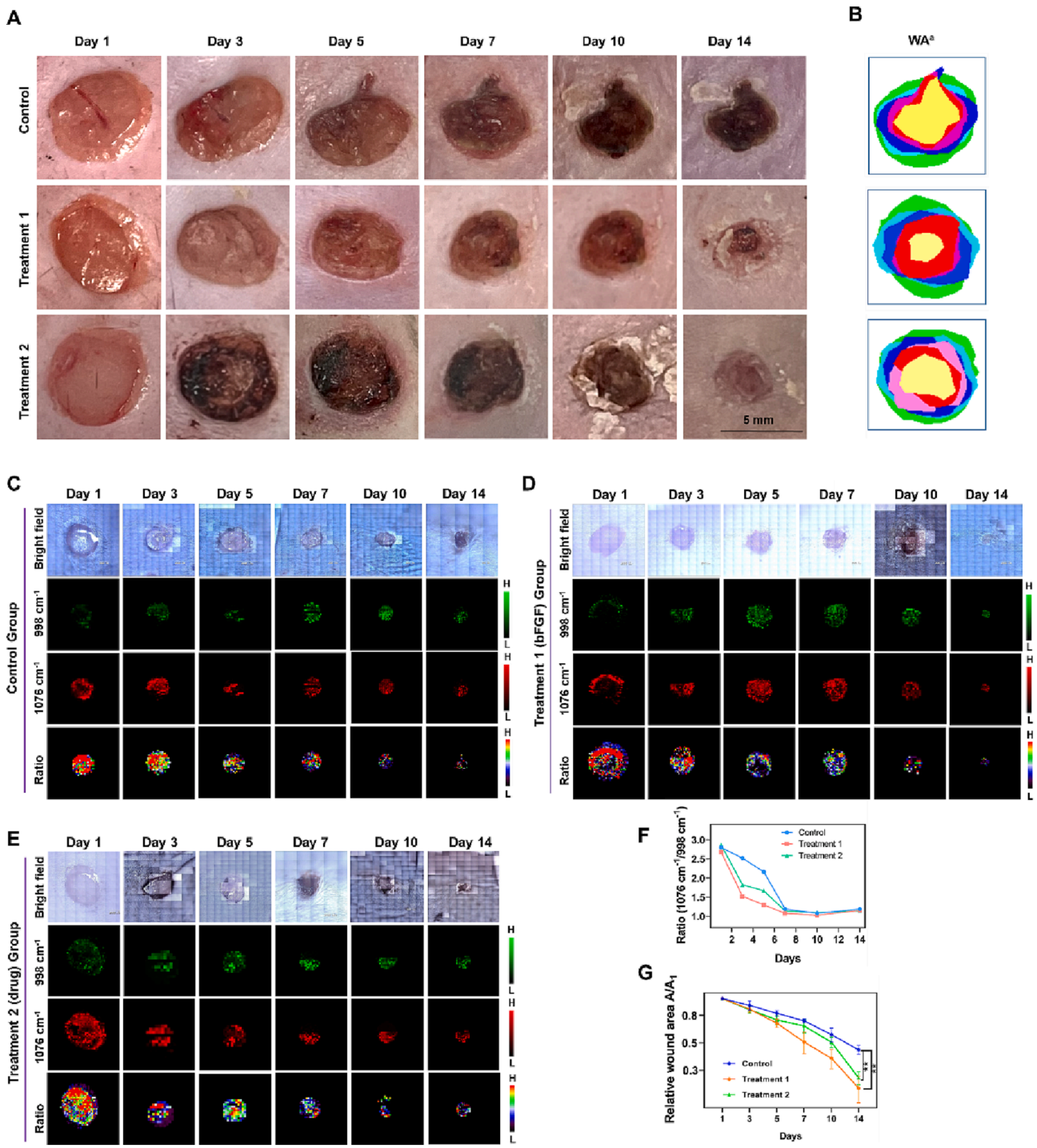

Fig. 6. (A) Representative photographic images of db/db mice with wounds in the groups of the untreated control, or treated with bFGF (treatment 1 group) and metformin + empagliflozin (treatment 2 group). (B) Simulation images of wound area in different groups. The green area meant the initial area and yellow area represented the wound area at 14 day. (C) - (E) Corresponding pseudo-color-coded in vivo SERS mapping images of the probe-applied wounds at up to 14 days without and with treatment. (F) and (G) Quantification of SERS intensity ratio and wound area of diabetic wounds after applying the probe in the control group, treatment 1 group and treatment 2 group, respectively. Wound SERS mapping was achieved using exposure time of 0.5 s (633 nm-laser power, 50 × objective). Statistical analysis was performed using one-way analysis of variance followed by post hoc Tukey multiple comparisons (n = 3, mean ± S. E. M., **P < 0.01).

inflammation levels (Fig. 6F). These in vivo results demonstrated that the proposed SERS probe could be probably used as a powerful tool to monitor the levels of $ONOO^-$ during the wounded healing process, thereby promote the development of detection technique.

3.6. Histological analysis and pilot toxicity evaluation

3-NT is produced by nitration between $ONOO^-$ and free tyrosine or tyrosine in the protein structure, which also aggravated the occurrence and development of diabetic vascular disease. CD31 and VEGF mediate the angiogenesis during the diabetic wound healing. Then, the

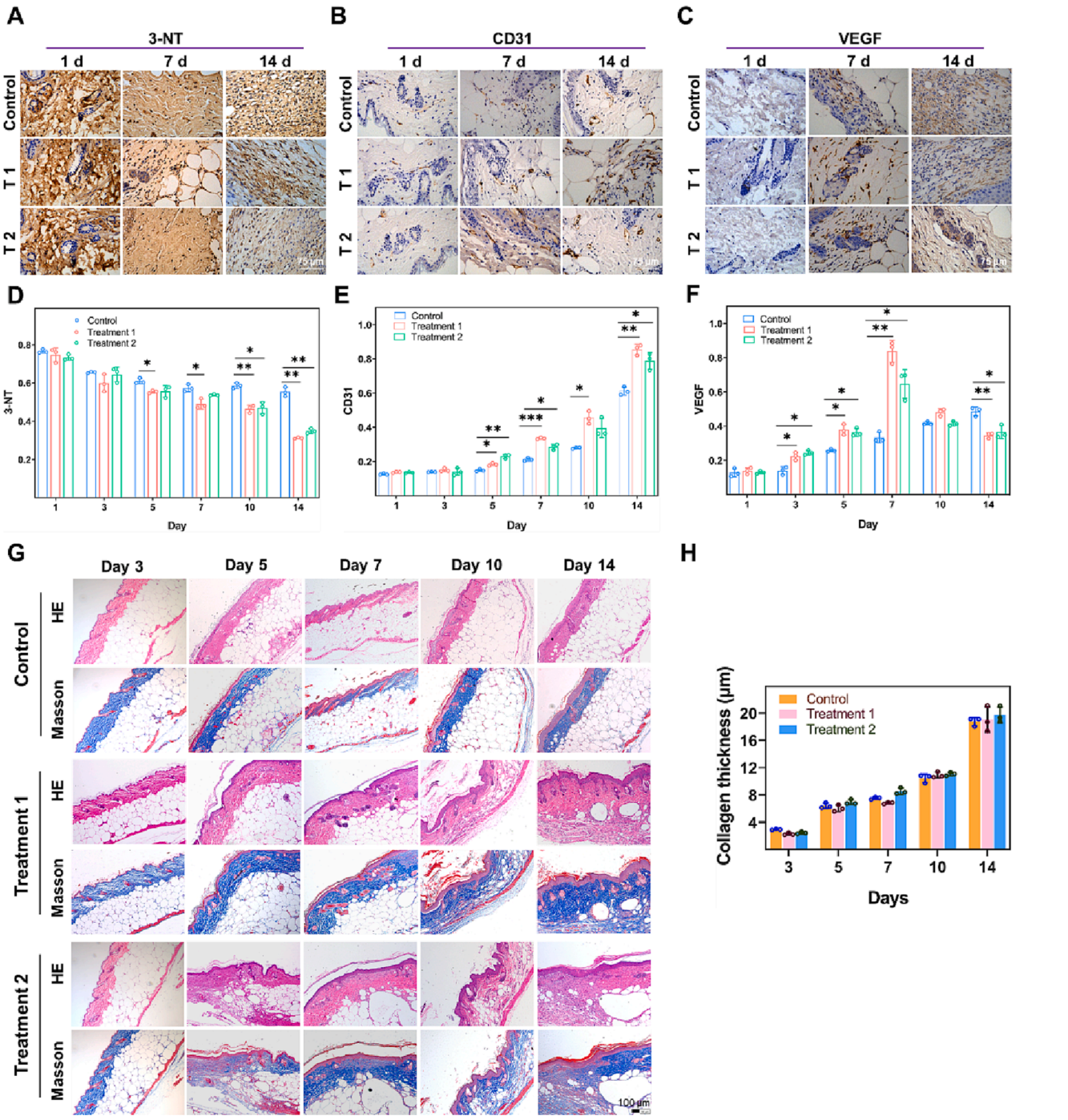

Fig. 7. Immunohistochemistry images of 3-NT (A), CD31 (B) and VEGF (C) of wounded skin tissues with and without treatment at different time points. Scale bar is 75 μm. (D) – (F) Quantification of immunohistochemistry images corresponding to (A) – (C). Three random view fields were selected under 40 × microscope and Image J software was used to calculate and count the mean OD values as the number of positive cells. (G) H&E and Masson staining of wounded skin tissues with and without treatment at different time points. (H) Quantification of Masson staining images of (G). Statistical analysis was performed using one-way analysis of variance followed by post hoc Tukey multiple comparisons (n = 3, mean ± S. E. M., *P < 0.05, **P < 0.01, ***P < 0.001).

immunohistochemistry (IHC) staining of 3-NT, CD31 and VEGF of the wounded skin tissues at 1st, 7th, and 14th day was performed to compare their expression under different conditions. The IHC images for each biomarker in three random visual fields were recorded under 40 × microscope as shown in Fig. 7A–C. The 3-NT expression exhibited the decreasing tendency in three groups, while the expression amount in control group was much higher than that of other groups, indicating the high concentration of $ONOO^-$. In addition, the expression in treatment 1 group was lower than that of treatment 2 group. CD31 expression in three groups indicated increasing amount and VEGF expression reached the maximum at 7th day, which demonstrated the angiogenesis promoting the wound healing.

In addition, the pathology of the wounded skin tissues was further evaluated by H&E and Masson staining (Fig. 7G). Pathological sections of three groups were collected on the 3rd, 5th, 7th, 10th and 14th day. The wound length of treatment 1 group was shorter than that of control group and treatment 2 group. Compared to the control group, more new granulation tissue and epidermis could be measured on the treatment 1

and treatment 2 groups. Furthermore, the collagen thickness during the healing process was counted (Fig. 7H), which increased in all groups with the progress time.

To further check the pilot toxicity of SERS nanoprobes, the levels of 3-NT, TNF-α, IL-1β and IL-6 in blood samples were tested, which were collected through tail vein at 1st, 3rd, 5th, 7th, 10th, and 14th day (Fig. S1). In the three groups, IL-1β exhibited much lower level at 14th day compared to the 1st day, indicating the decreasing inflammation. After constructing the wound skin models, the wounds would overexpressed ROS, which induced nitration of protein tyrosine residues to produce 3-NT. The expression level of 3-NT reached a high level on 5th day and decreased to the initial level on 14th day, confirming the dynamic fluctuations of $ONOO^-$ during the wound healing process. The inflammatory cytokines including TNF-α and IL-6 exhibited highest level and decreased to the low inflammatory level over time. Histological evaluation of major organs in Fig. S2, including heart, liver, spleen, lung, kidney and pancreas, indicated the normal function. These results suggested the excellent biocompatibility of SERS nanoprobes.

4. Conclusion

In summary, we explored a SERS imaging method using sensitive SERS nanoprobes for indication of $ONOO^-$ fluctuations at the single cell level and during the healing process of diabetic wound. Au@Ag core-ultrathin shell nanoparticles immobilizing phenylboronic pinacol ester were embedded with HS-PEG and BSA on the surface of Ag shell to achieve sensitive detection of $ONOO^-$ at single cell level and diabetic wound skin models. These results demonstrated that the proposed SERS nanoprobes exhibited high sensitivity, specificity and stability in the biological milieu. We believe that the detection of $ONOO^-$ fluctuations could broaden the applications of SERS imaging in biomedical research.

Declaration of Competing Interest

The authors declare that they have no known competing financial interests or personal relationships that could have appeared to influence the work reported in this paper.

Data availability

Data will be made available on request.

Acknowledgments

This work was supported by the National Natural Science Foundation of China (Grant No. 21864011, 22264013 and 21904030), Hainan Provincial Natural Science Foundation of China (Grant No. 820RC654), Natural Science Research Talent Project of Hainan Medical University (Grant No. JBGS202101), Hainan Province Clinical Medical Center (2021), Postgraduate Innovative Research Project of Hainan (Qhys2021-383), Nanhai Young-Talent Program of Hainan (Grant No. 20202007), Project for Functional Materials and Molecular Imaging Science Innovation Group of Hainan Medical University.

Appendix A. Supplementary data

Supplementary data to this article can be found online at https://doi.org/10.1016/j.cej.2023.144024.

References

[1] A.Y.Y. Cheng, M.B. Gomes, S. Kalra, A.-P. Kengne, C. Mathieu, J.E. Shaw, Applying the WHO global targets for diabetes mellitus, Nat. Rev. Endocrinol. 19 (4) (2023) 194–200.
[2] A. Soneja, M. Drews, T. Malinski, Role of nitric oxide, nitroxidative and oxidative stress in wound healing, Pharmacol. Rep. 57 (2005) 108–119.
[3] D. Duscher, E. Neofytou, V.W. Wong, Z.N. Maan, R.C. Rennert, M. Inayathullah, M. Januszyk, M. Rodrigues, A.V. Malkovskiy, A.J. Whitmore, G.G. Walmsley, M. G. Galvez, A.J. Whittam, M. Brownlee, J. Rajadas, G.C. Gurtner, Transdermal deferoxamine prevents pressure-induced diabetic ulcers, Proc. Natl. Acad. Sci. U.S. A. 112 (2015) 94–99.
[4] N.J. Trengove, M.C. Stacey, S. Macauley, N. Bennett, J. Gibson, F. Burslem, G. Murphy, G. Schultz, Analysis of the acute and chronic wound environments: the role of proteases and their inhibitors, Wound Repair Regen. 7 (6) (1999) 442–452.
[5] M.S. Brown, B. Ashley, A. Koh, Wearable technology for chronic wound monitoring: current dressings, advancements, and future prospects, Front. Bioeng. Biotechnol. 6 (2018) 47.
[6] Q.-X. Song, Y.i. Sun, K. Deng, J.-Y. Mei, C.J. Chermansky, M.S. Damaser, Potential role of oxidative stress in the pathogenesis of diabetic bladder dysfunction, Nat. Rev. Urol. 19 (10) (2022) 581–596.
[7] H. Batoko, V. Veljanovski, P. Jurkiewicz, Enigmatic translocator protein (TSPO) and cellular stress regulation, Trends Biochem. Sci. 40 (2015) 497–503.
[8] D. Baltzis, I. Eleftheriadou, A. Veves, Pathogenesis and treatment of impaired wound healing in diabetes mellitus: new insights, Adv. Ther. 31 (8) (2014) 817–836.
[9] H. Chen, Y. Guo, Z. Zhang, W. Mao, C. Shen, W. Xiong, Y. Yao, X. Zhao, Y. Hu, Z. Zou, J. Wu, Symbiotic algae-bacteria dressing for producing hydrogen to accelerate diabetic wound healing, Nano Lett. 22 (1) (2022) 229–237.
[10] Q. Zeng, X. Qi, G. Shi, M. Zhang, H. Haick, Wound dressing: from nanomaterials to diagnostic dressings and healing evaluations, ACS Nano 16 (2022) 1708–1733.
[11] D. Liu, S. Feng, G. Feng, A rapid responsive colorimetric and near-infrared fluorescent turn-on probe for imaging exogenous and endogenous peroxynitrite in living cells, Sensor Actuat. B-Chem. 269 (2018) 15–21.
[12] R. Ghosh, S. Debnath, A. Bhattacharya, P.B. Chatterjee, Affinity studies of hemicyanine derived water soluble colorimetric probes with reactive oxygen/nitrogen/sulfur species, ChemBioChem 24 (5) (2023) e202200541.
[13] K. Hu, Y. Li, S.A. Rotenberg, C. Amatore, M.V. Mirkin, Electrochemical measurements of reactive oxygen and nitrogen species inside single phagolysosomes of living macrophages, J. Am. Chem. Soc. 141 (11) (2019) 4564–4568.
[14] L. Li, Q. Liu, W. Fan, L. Ding, Z. Xue, X. Liu, X. Lu, A novel ratiometric electrochemical sensing strategy for monitoring of peroxynitrite anion released from high glucose-induced cells, Sensor Actuat. B-Chem. 328 (2021), 129071.
[15] P. Wang, L. Yu, J. Gong, J. Xiong, S. Zi, H. Xie, F. Zhang, Z. Mao, Z. Liu, J.S. Kim, An activity-based fluorescent probe for imaging fluctuations of peroxynitrite (onoo-) in the alzheimer's disease brain, Angew. Chem. Int. Ed. 61 (2022) e202206894.
[16] L. Wu, J. Liu, X. Tian, R.R. Groleau, B. Feng, Y. Yang, A.C. Sedgwick, H.-H. Han, Y. Wang, H.-M. Wang, F. Huang, S.D. Bull, H. Zhang, C. Huang, Y.i. Zang, J. Li, X.-P. He, P. Li, B.o. Tang, T.D. James, J.L. Sessler, Dual-channel fluorescent probe for the simultaneous monitoring of peroxynitrite and adenosine-5′-triphosphate in cellular applications, J. Am. Chem. Soc. 144 (1) (2022) 174–183.
[17] W.L. Cui, M.H. Wang, Y.H. Yang, J.Y. Wang, X. Zhu, H. Zhang, X. Ji, Recent advances and perspectives in reaction-based fluorescent probes for imaging peroxynitrite in biological systems, Coordin. Chem. Rev. 474 (2023), 214848.
[18] X. Luo, Z. Cheng, R. Wang, F. Yu, Indication of dynamic peroxynitrite fluctuations in the rat epilepsy model with a near-infrared two-photon fluorescent probe, Anal. Chem. 93 (4) (2021) 2490–2499.
[19] M. Ren, C. Zhou, L. Wang, X. Lv, W. Guo, Rationally designed meso-benzimidazole-pyronin with emission wavelength beyond 700 nm enabling in vivo visualization of acute-liver-injury-induced peroxynitrite, Chinese Chem. Lett. 34 (2023), 107646.
[20] N. Wang, H. Wang, J. Zhang, X. Ji, H. Su, J. Liu, J. Wang, W. Zhao, Endogenous peroxynitrite activated fluorescent probe for revealing anti-tuberculosis drug induced hepatotoxicity, Chinese Chem. Lett. 33 (3) (2022) 1584–1588.
[21] S.E.J. Bell, G. Charron, E. Cortés, J. Kneipp, M.L. de la Chapelle, J. Langer, M. Procházka, V. Tran, S. Schlücker, Towards reliable and quantitative surface-enhanced raman scattering (sers): from key parameters to good analytical practice, Angew. Chem. Int. Ed. 59 (2020) 5454–5462.
[22] M. Liebel, N. Pazos-Perez, N.F. van Hulst, R.A. Alvarez-Puebla, Surface-enhanced Raman scattering holography, Nat. Nanotech. 15 (12) (2020) 1005–1011.
[23] K. Xu, R. Zhou, K. Takei, M. Hong, Toward flexible surface-enhanced raman scattering (sers) sensors for point-of-care diagnostics, Adv. Sci. 6 (2019) 1900925.
[24] Y. Hang, J. Boryczka, N. Wu, Visible-light and near-infrared fluorescence and surface-enhanced Raman scattering point-of-care sensing and bio-imaging: a review, Chem. Soc. Rev. 51 (1) (2022) 329–375.
[25] D.W. Li, H.Y. Chen, Z.F. Gan, J.J. Sun, D. Guo, L.L. Qu, Surface-enhanced Raman scattering nanoprobes for the simultaneous detection of endogenous hypochlorous acid and peroxynitrite in living cells, Sensor Actuat. B-Chem. 277 (2018) 8–13.
[26] M. Masetti, H.-N. Xie, Ž. Krpetić, M. Recanatini, R.A. Alvarez-Puebla, L. Guerrini, Revealing DNA interactions with exogenous agents by surface-enhanced Raman scattering, J. Am. Chem. Soc. 137 (1) (2015) 469–476.
[27] R.A. Alvarez-Puebla, L.M. Liz-Marzán, SERS detection of small inorganic molecules and ions, Angew. Chem. Int. Ed. 51 (45) (2012) 11214–11223.
[28] J. Langer, D. Jimenez de Aberasturi, J. Aizpurua, R.A. Alvarez-Puebla, B. Auguié, J. J. Baumberg, G.C. Bazan, S.E.J. Bell, A. Boisen, A.G. Brolo, J. Choo, D. Cialla-May, V. Deckert, L. Fabris, K. Faulds, F.J. García de Abajo, R. Goodacre, D. Graham, A. J. Haes, C.L. Haynes, C. Huck, T. Itoh, M. Käll, J. Kneipp, N.A. Kotov, H. Kuang, E. C. Le Ru, H.K. Lee, J.-F. Li, X.Y. Ling, S.A. Maier, T. Mayerhöfer, M. Moskovits, K. Murakoshi, J.-M. Nam, S. Nie, Y. Ozaki, I. Pastoriza-Santos, J. Perez-Juste, J. Popp, A. Pucci, S. Reich, B. Ren, G.C. Schatz, T. Shegai, S. Schlücker, L.-L. Tay, K. G. Thomas, Z.-Q. Tian, R.P. Van Duyne, T. Vo-Dinh, Y. Wang, K.A. Willets, C. Xu,

H. Xu, Y. Xu, Y.S. Yamamoto, B. Zhao, L.M. Liz-Marzán, Present and future of surface-enhanced raman scattering, ACS Nano 14 (1) (2020) 28–117.
[29] H.-Y. Chen, D. Guo, Z.-F. Gan, L. Jiang, S. Chang, D.-W. Li, A phenylboronate-based SERS nanoprobe for detection and imaging of intracellular peroxynitrite, Microchim. Acta 186 (2018) 11.
[30] H.-Y. Chen, E. Kouadio Fodjo, L. Jiang, S. Chang, J.-B. Li, D.-S. Zhan, H.-X. Gu, D.-W. Li, Simultaneous detection of intracellular nitric oxide and peroxynitrite by a surface-enhanced raman scattering nanosensor with dual reactivity, ACS Sensors 4 (12) (2019) 3234–3239.
[31] X. Liu, C. Zhao, M. Zhuang, X. Meng, P. Zhang, G. Yang, Highly selective and sensitive surface-enhanced Raman scattering sensors for the detection of peroxynitrite in cells, Analyst 148 (10) (2023) 2256–2266.
[32] N.G. Bastús, J. Comenge, V. Puntes, Kinetically controlled seeded growth synthesis of citrate-stabilized gold nanoparticles of up to 200 nm: size focusing versus Ostwald ripening, Langmuir 27 (2011) 11098–11105.
[33] C. Qiu, W. Zhang, Y. Zhou, H. Cui, Y. Xing, F. Yu, R. Wang, Highly sensitive surface-enhanced Raman scattering (SERS) imaging for phenotypic diagnosis and therapeutic evaluation of breast cancer, Chem. Eng. J. 459 (2023), 141502.
[34] S. Matoori, A. Veves, D.J. Mooney, Advanced bandages for diabetic wound healing, Sci. Transl. Med. 13 (2021) eabe4839.
[35] M. Farahani, A. Shafiee, Wound healing: from passive to smart dressings, Adv. Healthc. Mater. 10 (16) (2021) 2100477.